4. Selected Research Activities

4.1. Lunar Studies

Yu. G. Shkuratov, V. G. Kaydash, V. V. Korokhin, N. N. Opanasenko, Yu. I. Velikodsky

The main goal of our optical investigations of the Moon is the prediction and mapping of chemical and mineral composition parameters of the lunar surface and its structure properties. For this purpose we use Clementine, Lunar Prospector, and Smart-1 data as well as data of laboratory measurements of lunar samples (LSCC data). Our studies also are devoted to photometric and polarimetric studies of the Moon with telescopes. We consider below several examples.

Phase-angle-ratio technique

The brightness of the lunar surface depends on the phase angle. This dependence, referred as the phase function, is controlled by the regolith structure at wide range of spatial scales. The phase function can be approximated with an exponential curve. Anomalies in the phase function (e.g., much variations of its steepness or exponent) indicate anomalies in the regolith structure. We use a series of 52 images of a vicinity of the Apollo-15 landing site taken with Clementine UVVIS camera in orbit 299 to retrieve information about regional distribution of the parameter characterizing the steepness that is the exponent. The spacecraft moved from South to North almost through the local zenith. The phase angle changed in the range of 26° – 55° through the series. The image taken almost from the zenith is shown in Fig. 11 a. The image resolution is about 200 m. The map of the phase function steepness is shown in Fig. 11 b. A contrasting shadow-like pattern of mountains (Apennines) and a channel (Rima Hadley) does not reflect real variations of the photometric function parameters and should be disregarded in the analysis. These strong variations are caused by relatively steep surface slopes which were not taken into account when we calculated the observation geometry. One can see several distinctive diffuse features on the flat mare surface. The most pronounced feature is a diffuse crater halo shown with the arrow B and C in Fig. 11 b. A small dark spot (right arrow A in Fig. 11 b) is not associated with any fresh crater but exactly coincides with the Apollo 15 landing site. The anomaly is related to damages of the regolith structure around the landing site; it is probably caused with the lander jets. In addition, using another data, the anomalies were found for fresh lunar craters and some volcanic edifices. In the latter case the anomalies are due to pyroclastic deposits.

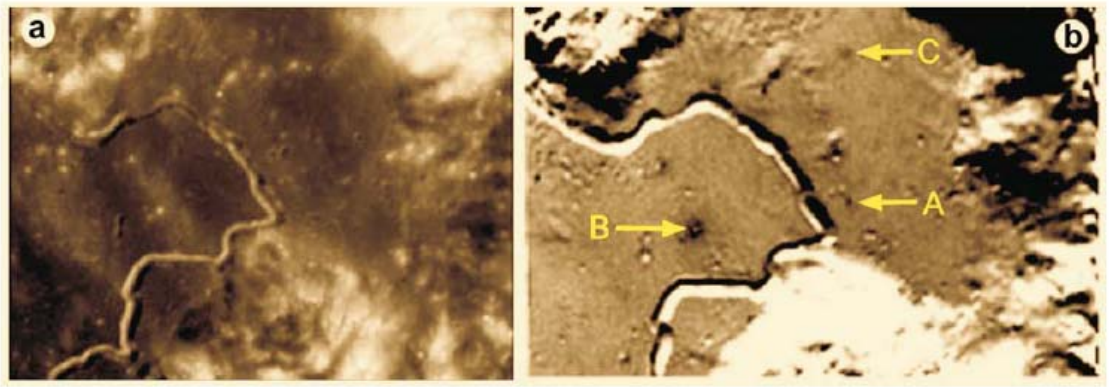

Figure 11. Image of Apollo-15 landing region (a). Rima Hadley is clearly seen. Brighter shades denote higher steepness of brightness phase curve (b). Arrows A, B, and C) show the landing site and young craters.

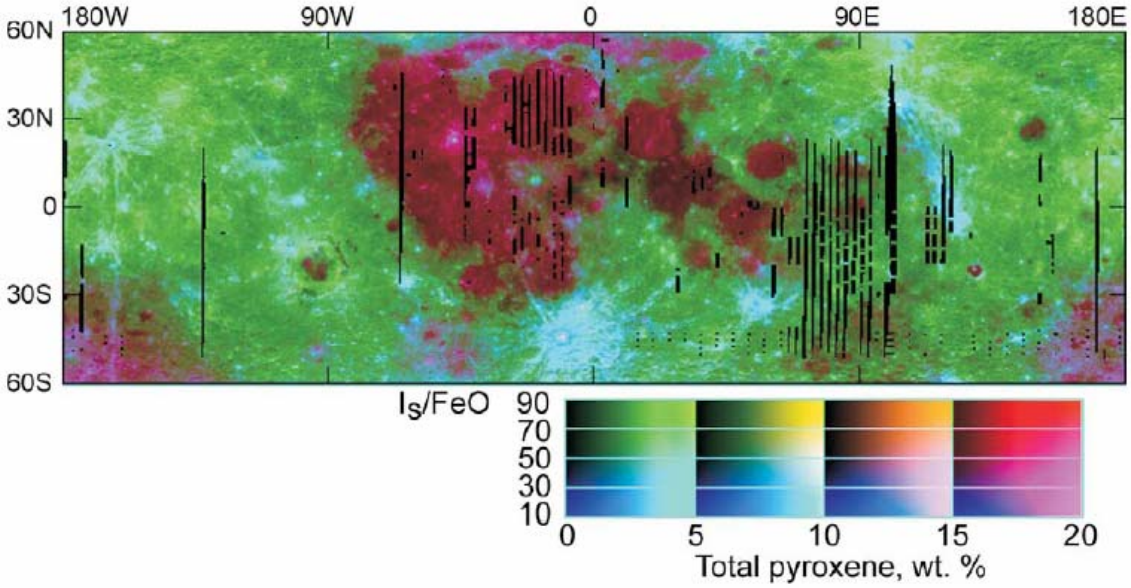

Figure 12. Two-parametric map of the maturity degree and total pyroxene abundance of the lunar surface.

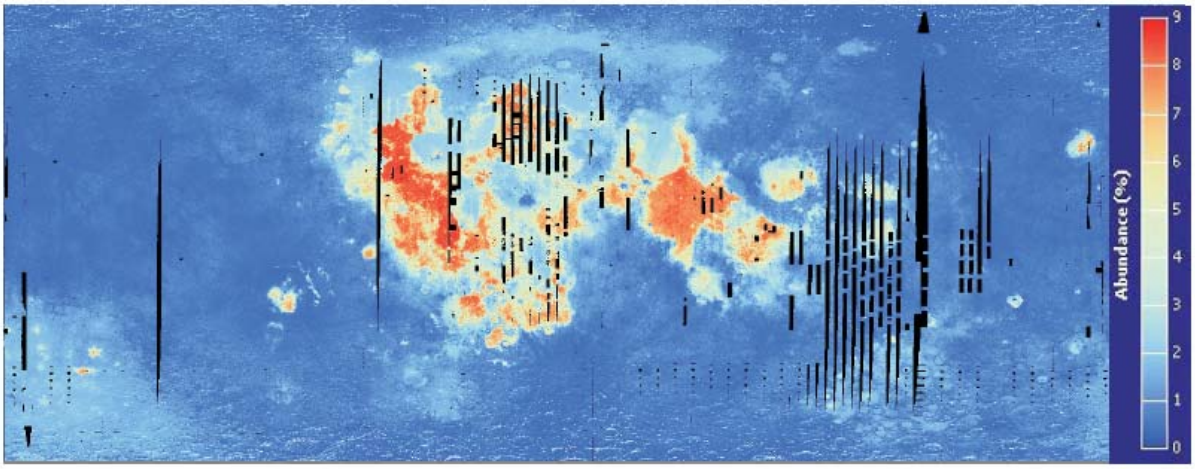

Figure 13. Distribution of TiO_2 over the lunar surface mapped using Clementine mosaics with application of artificial neural networks to analysis of correlations between optical and chemical characteristic of lunar samples (LSCC data)

Mapping of surface composition

A new approach for remote sensing determination of the lunar surface composition has been proposed in our Institute. The technique uses Clementine UVVIS data and results of spectral and chemical/mineral studies of lunar samples by the Lunar Soil Characterization Consortium [Pieters et al. Icarus 2002, 155, 285]. The main rock-forming oxides (FeO, TiO_2, Al_2O_3), minerals (pyroxene, plagioclase), and maturity degree (I_s/FeO) were mapped with 1 km resolution. To map chemical/mineral parameters of the lunar surface we use images acquired in the following four Clementine UVVIS camera spectral bands: 415, 750, 900, and 1000 nm. The correlations between the linear combinations of albedo measured in the mentioned spectral bands and chemical/mineral characteristics for lunar 52 samples allow prognosis lunar maps of the characteristics. An example of applying such a technique is presented in Fig. 12 that is a lunar two-parameter map of the maturity degree, I_s/FeO, and total pyroxen content in lunar soil. The parameter I_s/FeO is the ratio of ferromagnetic resonance intensity I_s (which is proportional to metallic iron content) to the total Fe content. It is closely related to the age (exposition time) of the lunar surface. Our analysis shows that the regoliths of morphologically young craters are characterized with low degree of maturity and high content of pyroxene. Small areas with anomalous high maturity degree are found. They are mainly located at the center of the lunar nearside and associated with so-called dark mantle deposits.

We also have suggested a technique to determine the chemical and mineral composition of the lunar surface using artificial neural networks (ANN). We demonstrate this powerful non-linear approach for prognosis of TiO_2 abundance (see Fig. 13) using the Clementine UVVIS mosaics and Lunar Soil Characterization Consortium data. The ANN technique allows one to study correlations between spectral characteristics of lunar soils and composition parameters without any restrictions on the character of these correlations.

The results obtained could be useful for the strategy of analysing lunar data that will be acquired in incoming lunar missions especially in case of the Chandrayaan-1 and Lunar Reconnaissance Orbiter missions.

Polarimetric studies

Polarimetric investigations of the Moon have a long history. They are not being actively pursued. One reason is that at large phase angles there is an inverse correlation between albedo *A* and polarization degree P of light scattered by the lunar surface. This effect is often called Umov's law. The correlation is approximately linear on a log-log

scale: log$P$ + $a$log$A$ = b, where a and b are constants. The correlation coefficient is up to 0.95. Because of this correlation, mapping polarization degree often is considered as non-informative for remote sensing of the lunar surface.

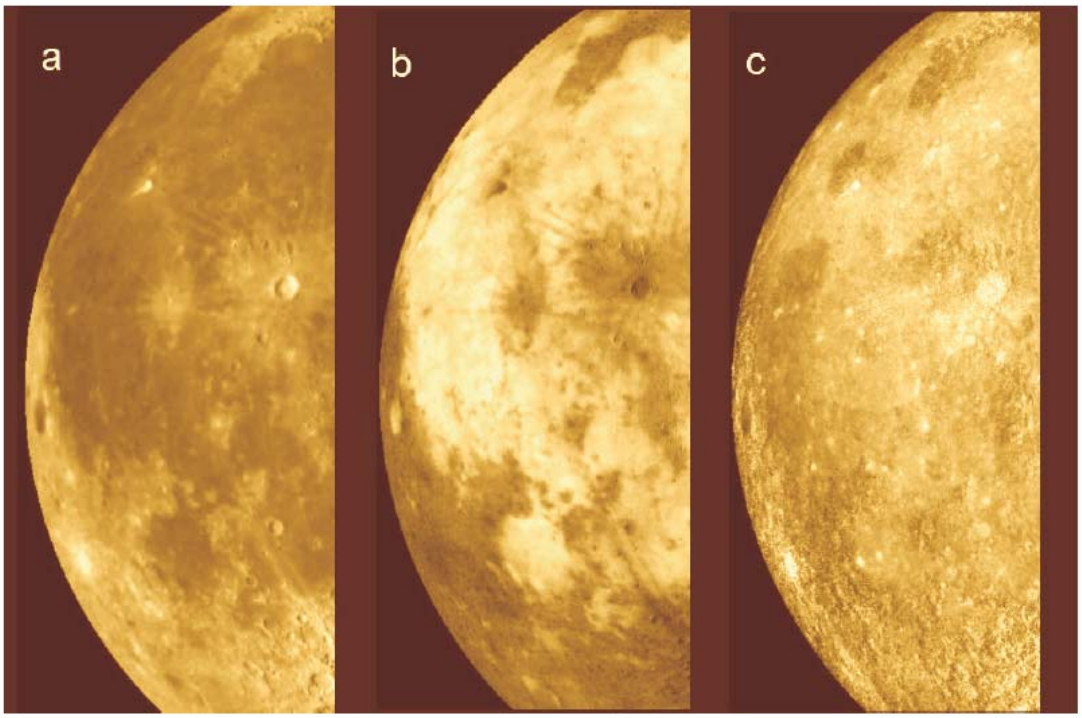

Figure 14. Image of west portion of the Moon with compensation of longitude and latitude dependence of brightness – (a), distribution of linear polarization degree at phase angle 88° – (b), distribution of the parameter b = log AP^{a}_{max} – (c)

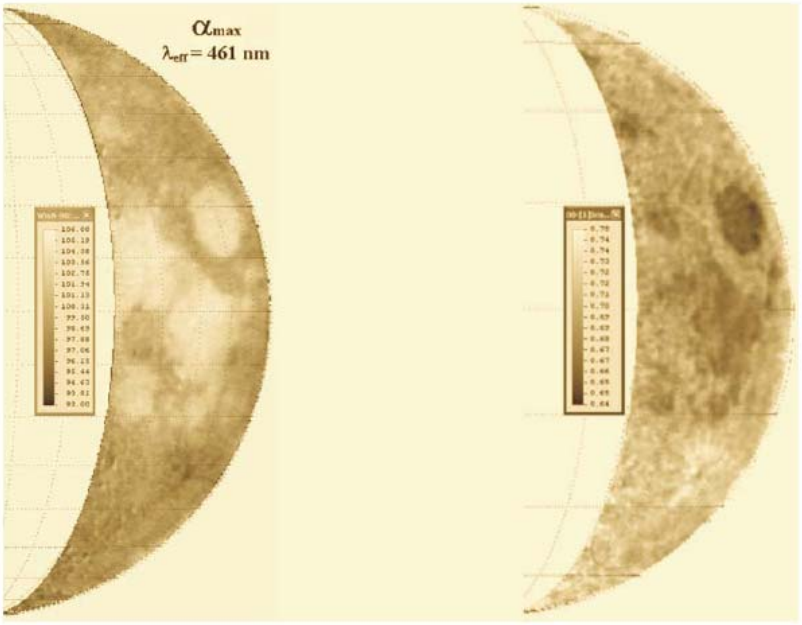

Figure 15. Mapping the position of the maximum of positive polarization $\alpha_{max}(\lambda_{eff}$=461 nm). East portion of the Moon

Figure 16. Mapping the ratio P_{max}(670 nm)/P_{max}(460 nm). East portion of the lunar nearside

First attempts to acquire further information from polarization have been undertaken in Kharkiv observatory by quantifying the deviation of the polarization from the regression line of the albedo correlation. To characterize the deviations, the parameter $(P_{max})^a A$ has been proposed. It has been shown that the parameter bears significant information on the characteristic size and microporosity of the lunar regolith. Analysis of the images of the distribution of $(P_{max})^a A$ shows the following (see Fig. 14): (1) rayed young craters including the Aristarchus crater have increased values of the parameter, perhaps because of the immature character of the regolith (coarse grains); and (2) regions characterized by decreased values of $(P_{max})^a A$, e.g., Aristarchus Plateau and Marius Hills area that are regions of volcanism that could be accompanied by ash deposits containing fine (dust) particles. Figure 14 a shows an image of the lunar albedo for the western portion of the lunar nearside. The image has been obtained at the wavelength 0.43 μm. The brightness trend from the lunar limb to the terminator has been compensated. Figure 14 b shows the distribution of the degree of linear polarization that is very similar to an albedo negative of Figure 14 a, owing to that there is the inverse correlation between albedo and polarization degree. Figure 14 c is the image demonstrating the distribution of the parameter $(P_{max})^a A$. Laboratory measurements of lunar samples and size-particle separates of terrestrial glasses have shown that the variations of this parameter are closely correlated with the particle size. Young craters are clearly visible in Fig. 14 c indicating their coarse regolith particles.

Polarimetric observations of the lunar surface with an imaging CCD–polarimeter were carried out at 23 phase angles, from 8° to 123°. The values of positive polarization degree maximum P_{max} and its phase angle α_{max} in two spectral bands, λ_{eff} = 461 nm and λ_{eff} = 669 nm, for the east portion of the lunar nearside have been mapped. Examples of mapping the parameters of maximum polarization: (a) α_{max} at λ_{eff} = 461 nm and (b) Cp_{max} = P_{max}(669 nm) / P_{max}(461 nm) are shown in Fig. 15. As can be seen the parameter α_{max} and albedo of the lunar surface anticorrelate with each other. The correlation diagram "Cp_{max} – albedo" shows that there is an anticorrelation for mares and direct correlation for highlands. The histogram of P_{max} distribution over the portion of the lunar disk has a distinct maximum at P_{max} = 7.3 % for λ_{eff} = 461 nm and that at P_{max} = 5.25 % for λ_{eff} = 669 nm. The range of P_{max} variations is 4.0 ... 21.0 % for λ_{eff} = 461 nm and 3.0 ... 15.0 % for λ_{eff} = 669 nm. The histogram of α_{max} distribution is distinctly bimodal with the first peak at α = 99.7° (highlands), and the second one at α = 104.1° (mares) for λ_{eff} = 461 nm. For λ_{eff} = 669 nm we have α = 96.8° and α = 101.2°, respectively. The histogram is narrower in blue

light, 94.0° ... 106.0°, as compared to that in red light (90.0° ... 105.0°). The maximum of polarization occurs at larger phase angles in the blue band.